PUBLICATION

MUSTANG

A MUltiple Space and Time scale Approach for the quaNtification of deep saline formations for CO_2 storaGe

Project Number:227286

AUTHORS: *Marco Dentz, Philippe Gouze, Anna Russian, Jalal Dweik, Frederick Delay*

TITLE: *Diffusion and trapping in heterogeneous media: An inhomogeneous continuous time random walk approach*

The research leading to these results has received funding from the European Community's Seventh Framework Programme [FP7/2007/2013) under grant agreement n° [227286]

Status	AUTHOR VERSION
Date	2012
Publisher	Science Direct
Reference	Advances in Water Resources, Vol. 49, pp. 13-22, 2012

Diffusion and Trapping in Heterogeneous Media: An Inhomogeneous Continuous Time Random Walk Approach

Marco Dentz

Institute of Environmental Assessment and Water Research (IDÆA), Spanish National Research Council (CSIC), 08034 Barcelona, Spain

Philippe Gouze

Géoscience, Université de Montpellier 2, CNRS, Montpellier, France

Anna Russian

Institute of Environmental Assessment and Water Research (IDÆA), Spanish National Research Council (CSIC), 08034 Barcelona, Spain

Jalal Dweik

Géoscience, Université de Montpellier 2, CNRS, Montpellier, France

Frederick Delay

Laboratoire d'Hydrologie et de Géochimie de Strasbourg, Université de Strasbourg, Strasbourg, France.

Abstract

We study diffusion in a heterogeneous medium that is characterized by spatially varying diffusion properties from a random walk point of view. We show that an inhomogeneous continuous time random walk (CTRW) with a spatially variable exponential transition time distribution solves the spatially discretized heterogeneous diffusion equation. This demonstrates the equivalence of the widely used time-domain random walk (TDRW) scheme and spatially inhomogeneous CTRW and at the same time provides a demon-

stration of the formal equivalence of the TDRW particle formulation and the heterogeneous diffusion equation. Based on this equivalence, we develop a TDRW method for heterogeneous diffusion under spatially variable multirate mass transfer properties. We discuss the implementation of these schemes and study the diffusion behavior in the presence of traps that are characterized by a truncated power-law trapping time distribution.
Keywords: Diffusion in Random Media, Continuous Time Random Walks, Time-Domain Random Walks, Multirate Mass Transfer, Stochastic Modeling

1. Introduction

Diffusion in heterogeneous media is a ubiquitous process in nature that describes a range of different physical phenomena [1, 2, 3] including chemical transport in low permeability media such as clays and granites [4] and in general in immobile regions of a heterogeneous porous medium [5], Darcian fluid flow through heterogeneous media, heat transport and electric current through a conductor [6, 7, 8], as well as diffusion in biological systems [9].

The present work is motivated through the diffusion of chemicals in heterogeneous low permeability media that are characterized by spatially varying diffusion properties. The concentration $c(\mathbf{x}, t)$ of a dissolved chemical satisfies the diffusion equation

$$\phi(\mathbf{x})\frac{\partial c(\mathbf{x}, t)}{\partial t} = \nabla \cdot [D(\mathbf{x})\nabla c(\mathbf{x}, t)], \tag{1}$$

in which $\phi(\mathbf{x})$ is porosity and $D(\mathbf{x})$ the diffusion coefficient, which in general depends on porosity [e.g., 10]. As a side note, for the case of the flow

of an incompressible fluid through a porous medium, $\phi(\mathbf{x})$ would denote specific storativity, $D(\mathbf{x})$ hydraulic conductivity and $c(\mathbf{x}, t)$ hydraulic head. The diffusion equation (1) for heterogeneous media does not have a general closed form solution and is often approached analytically using perturbation methods [7, 6, 3], and numerically using finite difference, finite element or finite volume methods [11, 12]. In this paper, we focus on numerical approaches based on random walk particle tracking [13, 7]. This numerical method is based on the fact that equation (1) is equivalent to the Langevin equation [e.g., 5]

$$\frac{d\mathbf{x}(t)}{dt} = \frac{\nabla D[\mathbf{x}(t)]}{\phi[\mathbf{x}(t)]} + \sqrt{2\frac{D[\mathbf{x}(t)]}{\phi[\mathbf{x}(t)]}}\boldsymbol{\xi}(t), \tag{2}$$

in which $\mathbf{x}(t)$ describes the trajectories of the 'solute' particles that constitute the concentration distribution $c(\mathbf{x}, t)$. In fact, $c(\mathbf{x}, t)$ is expressed in terms of the particle trajectory as [14]

$$c(\mathbf{x}, t) = \phi(\mathbf{x}) \left\langle \delta[\mathbf{x} - \mathbf{x}(t)] \right\rangle, \tag{3}$$

in which $\delta(\mathbf{x})$ denotes the d-dimensional Dirac delta-distribution. The numerical solution of the Langevin equation (2) can be very costly because the heterogeneous diffusion properties may require a fine time-discretization in order to ensure that a particle actually 'sees' the spatial variability [e.g., 15, 4]. There may be inaccuracies because in some regions of the medium with little variability a coarse discretization is sufficient while in regions with high variability a fine time discretization is required [15]. Also, as pointed out by McCarthy [8] in regions of small diffusivity a particle may have to wait at a given site for a large number of simulation steps, which is inefficient. Furthermore, for pixelized maps of heterogeneous media as obtained

by X-ray microtomography (XMT) [4, 5], see Figure B.1, diffusion properties are spatially discontinuous, which makes the use of Eq. (2) complicated because it relies on the calculation of the gradient of the diffusion coefficient $D(\mathbf{x})$ (see for example [16]).

In order to avoid these problems, particle schemes were proposed that rely on spatial increments, whose absolute values are deterministic, combined with random time increment [8, 17, 18, 15, 4, 19]. That is, at each random walk step the particle moves a given distance (which can be given by the pixel size of the discretized medium representation, for example) in a random direction, whose probability is calculated from the diffusion properties of the medium. The time for the step is random, which reflects the stochastic nature of the diffusion process. There has been in fact a certain ambiguity on how to model the distribution of transition time. In [8], [18] and [4], for example, an exponential transition time distribution is employed, while [15] and [20] use a lognormal transition time distribution. Ref. [19] identifies the transition time with the first-passage time to cross a certain distance by diffusion. The different variants of this methodology have been called continuous time random walk (CTRW) on random media [8, 18] and time-domain random walk (TDRW) [17, 15]. In the different aforementioned applications, TDRW method has been used for the determination of effective diffusivity [4], effective hydraulic and electrical conductivity [8], for the upscaling of fluid flow in fractured rocks [18] and for the efficient simulation of chemical transport in fracture networks [20, 21].

The TDRW method is closely related to the continuous time random walk (CTRW) framework [22, 23]. A CTRW describes the stochastic movement

of particles as random walk in space and time. The CTRW approach has been used for the modeling of electron transport in disordered media [23], diffusion in turbulence [24], chemical transport in heterogeneous porous media, to name but a few, see also the exhaustive review paper by Berkowitz et al. [25]. It has been used successfully to model anomalous transport features in fluctuating environments. In this context it can be seen as an average transport framework that is based on the observation that, when looking at average Lagrangian transport dynamics, particles may need different times to cross the same distance, due to heterogeneous medium properties. Effective particle dynamics can be described as a CTRW. This is the reason why CTRW is often referred to as an ensemble averaged transport model. Strictly speaking, it is a model that describes particle movements as a random walk in space and time coordinates. As pointed out above, McCarthy [8] and Noetinger and Estebenet [18] refer to TDRW as a CTRW method because the time increment is random. The papers on TDRW, we reviewed above, propose a TDRW algorithm as an efficient solution methodology for the heterogeneous diffusion equation. However, in none of these papers, have we found a demonstration of the formal equivalence of the TDRW algorithm and the diffusion equation, as it exists for the equivalence of the diffusion equation (1) and the Langevin equation (2).

In this paper, we show the equivalence of the TDRW scheme and the heterogeneous diffusion problem (1) using the framework of inhomogeneous CTRWs. The constructive nature of this demonstration sheds new light on the foundations of the TDRW approach and allows for the generalization of the TDRW method to diffusion under heterogeneous mobile immobile trans-

port. We discuss the numerical implementation of the method and present numerical examples that study diffusion and trapping in heterogeneous media.

2. Theoretical Development

In this section, we first consider a continuous time random walk (CTRW) [22, 23, 25] on an inhomogeneous spatial lattice, which is characterized by non-stationary spatial transition probabilities and space-dependent transition time distribution [26, 27, 28]. We then show that the inhomogeneous CTRW with an exponential transition time distribution solves the discrete equations that describe diffusion in heterogeneous media. This demonstrates the equivalence of the time-domain random walk (TDRW) scheme, which was developed for the solution of heterogeneous diffusion problems [8, 18, 4], and CTRW. Based on these results, we discuss an extension of the TDRW method for heterogeneous diffusion in combination with heterogeneous trapping properties.

2.1. Spatially Inhomogeneous CTRW

We consider a spatially inhomogeneous continuous time random walk (CTRW) [e.g., 22, 23] on a lattice defined by the following set of recursion equations

$$\mathbf{x}_i(n+1) = \mathbf{x}_j(n) + \boldsymbol{\xi}_{ij}, \qquad t_{n+1} = t_n + \theta_j, \tag{4}$$

where the position of lattice point j is denoted by $\mathbf{x}_j$. The probability for a spatial transition ξ_{ij} between points j and i (i.e. from j to i) is given by w_{ij}, the probability density of the random time increment θ_j depends on the

position of the particle at step n. Its distribution is given by the transition time density $\psi_j(t)$. Equation (4) describes an inhomogeneous CTRW because the probabilities w_{ij} and $\psi_j(t)$ for spatial and temporal particle transitions depend on the particle positions within the lattice.

The particle density $g_i(t)$ at point i is defined by

$$g_i(t) = \langle \Delta[\mathbf{x}_i - \mathbf{x}_j(t)] \rangle \,. \tag{5}$$

The angular brackets denote the average over all particles that are launched in the random walk (4) and the function $\Delta[\mathbf{x}_i - \mathbf{x}_j(t)]$ is 1 if $\mathbf{x}_j(t) = \mathbf{x}_i$ and zero otherwise. The random walk (4) describes time as a stochastic process. The number of steps needed to reach time t is counted by the renewal process $n_t = \max(n|t_n \leq t)$. The number density $g_i(t)$ then reads in terms of the space-time particle trajectories (4) as

$$g_i(t) = \langle \Delta[\mathbf{x}_i - \mathbf{x}_j(n_t)] \rangle \,. \tag{6}$$

This expression can be expanded as

$$g_i(t) = \sum_{n=0}^{\infty} \langle \Delta[\mathbf{x}_i - \mathbf{x}_j(n)] \delta_{n,n_t} \rangle \,. \tag{7}$$

The statement $n = n_t$ is equivalent to $0 \leq t - t_n < \theta_i$. This condition can be expressed by the impulse function $\mathbf{I}_{B_i}(t)$, which is 1 for $t \in B_i = [0, \theta_i[$ and zero otherwise. Thus, we can write $g_i(t)$ as

$$g_i(t) = \sum_{n=0}^{\infty} \langle \Delta[\mathbf{x}_i - \mathbf{x}_j(n)] \mathbf{I}_{B_i}(t - t_n) \rangle \,. \tag{8}$$

By inserting a Dirac-delta, we obtain

$$g_i(t) = \sum_{n=0}^{\infty} \int_0^t dt' \, \langle \Delta[\mathbf{x}_i - \mathbf{x}_j(n)] \delta(t' - t_n) \rangle \, \langle \mathbf{I}_{B_i}(t - t') \rangle \,. \tag{9}$$

We could break the noise average because of the Markovianity of the process (4). Executing the second average explicitly and defining $R_i(t) = \sum_{n=0}^{\infty} \langle \Delta[\mathbf{x}_i - \mathbf{x}_j(n)] \delta(t - t_n) \rangle$, we obtain

$$g_i(t) = \int_0^t dt' R_i(t') \int_{t-t'}^{\infty} d\tau \psi_i(\tau). \tag{10}$$

The $R_i(t)$ describes the probability per time for the particle to just arrive at $\mathbf{x}_i$ at time t. From the Markovianity of the process (4) we obtain for $R_i(t)$ that

$$R_i(t) = \rho_i \delta(t) + \sum_{[ik]} w_{ik} \int_0^t dt' \psi_k(t - t') R_k(t'), \tag{11}$$

with $\rho_i = g_i(t = 0)$ the initial particle density at point $\mathbf{x}_i$. Notice that (11) is a Chapman-Kolmogorov type equation that describes the probability to just arrive at $\mathbf{x}_i$ at time t as the sum over all possible transitions from a position $\mathbf{x}_k$ to $\mathbf{x}_i$ of duration $t - t'$. The notation $\sum_{[ik]}$ indicates summation over nearest neighbors of pixel i. Combination of (10) and (11) in Laplace space gives for the Laplace transform of $g_i(t)$ the well known generalized Master equation [e.g., 29]

$$\lambda g_i^*(\lambda) = \rho_i + \sum_{[ik]} \frac{w_{ik} \lambda \psi_k^*(\lambda)}{1 - \psi_k^*(\lambda)} g_k^*(\lambda) - \frac{\lambda \psi_i^*(\lambda)}{1 - \psi_i^*(\lambda)} g_i^*(\lambda). \tag{12}$$

The Laplace transform is defined in [30]. Here and in the following, Laplace transformed quantities are marked by an asterisk, the Laplace variable is denoted by λ.

2.2. Equivalence with Heterogeneous Diffusion

In order to establish the equivalence between the inhomogeneous CTRW detailed in in the previous section and the heterogeneous diffusion equa-

tion (1), we consider the exponential transition time density [25]

$$\psi_j(t) = \tau_j^{-1} \exp(-t/\tau_j). \tag{13}$$

Inserting the Laplace transform of (13) into (12) gives

$$\lambda g_i^*(\lambda) = \rho_i + \sum_{[ij]} w_{ij} \tau_j^{-1} g_k^*(\lambda) - \tau_i^{-1} g_i^*(\lambda). \tag{14}$$

Transforming this equation back to real time, we obtain the Master equation

$$\frac{\partial g_i}{\partial t} = \sum_{[ij]} w_{ij} \tau_j^{-1} g_j - \tau_i^{-1} g_i. \tag{15}$$

We now define the transition probabilities w_{ij} and transition times τ_j as

$$w_{ij} = \frac{b'_{ij}}{\sum_{[jk]} b'_{kj}}, \qquad\qquad \tau_j = \frac{1}{\sum_{[kj]} b'_{kj}}, \tag{16}$$

where the b'_{ij} are defined below. By definition the w_{ij} fulfill the normalization condition $\sum_{[ji]} w_{ij} = 1$. Inserting these definitions into (15), we obtain

$$\frac{\partial g_i}{\partial t} = \sum_{[ij]} b'_{ij} g_j - \sum_{[ki]} b'_{ki} g_i. \tag{17}$$

Notice that for $b'_{ij} = b'_{ji}$, this equation describes diffusion on a lattice with symmetric barriers [e.g., 31].

To establish the equivalence of the Master equation (17) and the diffusion equation (1), we need to further specify the b'_{ij} in terms of the medium porosity and diffusion coefficients. Thus, we define now

$$b'_{ij} = \frac{b_{ij}}{V_j \phi_j}, \qquad\qquad b_{ij} = \frac{S_{ij} \hat{D}_{ij}}{\xi_{ij}}, \tag{18}$$

where V_j and ϕ_j are volume and porosity of pixel j, respectively, S_{ij} denotes the surface area between pixels i and j and $\hat{D}_{ij}$ is an average diffusion

coefficient between pixels i and j, see Section 3.1. Notice that the b_{ij} are symmetric by definition, while the b'_{ij} and thus the transition probabilities w_{ij} are in general not. Furthermore, we define the rescaled particle density

$$c_i = \frac{g_i}{V_i \phi_i}. \tag{19}$$

Inserting (18) and (19) into (17) gives

$$V_i \phi_i \frac{\partial c_i}{\partial t} = \sum_{[ij]} b_{ij} c_j - \sum_{[ij]} b_{ij} c_i. \tag{20}$$

This equation together with definition (18) of the b_{ij} corresponds to a finite volume discretization of (1) as outlined for example in [4]. The quantity c_i is identified with the solute concentration in the fluid phase. Thus, in the limit $\xi_{ij} \to 0$, we obtain the heterogeneous diffusion equation (1). This establishes the equivalence between (1) and the CTRW scheme (4) for the transition probabilities w_{ij} and mean transition times τ_j defined as

$$w_{ij} = \frac{b_{ij}}{\sum_{[jk]} b_{kj}}, \qquad \tau_j = \frac{V_j \phi_j}{\sum_{[kj]} b_{kj}}, \tag{21}$$

where we used (18) in (16). Notice that the random walk algorithm based on (4) and (16) for the exponential $\psi_i(t)$ (13) is identical to the time domain random walk (TDRW) presented by [4]. Delay et al. [4] deduced the exponential transition time distribution (13) by interpreting (20) in terms of single particle transitions. This explicit demonstration, removes ambiguity with respect to the distribution of transition times.

2.3. Heterogeneous Diffusion With Multirate Mass Transfer (MRMT)

In the previous section we established the equivalence between the spatially discrete heterogeneous diffusion equation (1) and the inhomogeneous

CTRW (4) with (13) and (21), or in other words, a TDRW. Here we consider the generalization of this framework to heterogeneous diffusion combined with multirate mass transfer (MRMT). The MRMT approach [e.g., 32, 33] describes transport in the presence of traps, or immobile zones, in which the solute can be immobilized for a certain amount of time. The trapping mechanisms may be chemical such as adsorption, or physical, such as very slow diffusion. It has been shown in Refs. [34] and [35] that the CTRW and multirate mass transfer modeling approaches are equivalent under certain conditions. Thus, based on these results and on the observation that a TDRW describes an inhomogeneous CTRW, we develop in the following a TDRW approach that models particle transport in heterogeneous media under spatially varying diffusion and trapping properties.

As in the previous section, we start with the formulation of MRMT as an inhomogeneous CTRW. We then consider the corresponding generalized Master equation and establish the equivalence to the spatially heterogeneous diffusion equation with spatially variable mass transfer. Linear multirate sorption-desorption and in general linear multirate mass transfer can be modeled in the framework of CTRW by introducing a trapping time distribution $p(t)$ [e.g., 36]. The particle transition time then is given by the time spent in the mobile domain and the sum of trapping times during a transition. The transition time distribution $\psi(t)$ with traps then is given in terms of the transition time distribution $\psi_0(t)$ without traps as [36]

$$\psi^*(\lambda) = \psi_0^*\left(\lambda + \alpha\left[1 - p^*(\lambda)\right]\right), \tag{22}$$

in which α is the trapping frequency during a transition. Benson and Meerschaert [35] studied the case for which the transition time without traps is

exponentially distributed using random walk particle tracking. A similar approach was used by Delay and co-workers [20, 37] to extend the TDRW method to account for matrix diffusion in the context of transport in fractured media.

Here, we consider the general case that the trapping time distribution $p_j(t)$ and trapping frequency α_j depend on position. Using the Laplace transform of the exponential distribution (13) for $\psi_0^*(t)$ in (22), we obtain for the $\psi_j(t)$ of heterogeneous diffusion and MRMT the expression

$$\psi_j^*(\lambda) = \frac{1}{1 + \lambda\tau_j + \alpha_j\tau_j[1 - p_j^*(\lambda)]}. \tag{23}$$

Inserting this explicit form in the generalized Master equation (12) gives

$$\begin{aligned}\lambda g_i^*(\lambda) = \rho_i + \sum_{[ik]} \frac{w_{ik}\lambda g_k^*(\lambda)}{\lambda\tau_k + \alpha_k\tau_k[1 - p_k^*(\lambda)]} \\ - \frac{\lambda g_i^*(\lambda)}{\lambda\tau_i + \alpha_i\tau_i[1 - p_i^*(\lambda)]}.\end{aligned} \tag{24}$$

In order to obtain the partial differential equation that governs transport under heterogeneous MRMT, we identify the w_{ik} in (24) with

$$w_{ik} = \frac{b_{ik}\tau_k}{V_k\phi_k}, \tag{25}$$

where we used (16) and (18). Furthermore, we set $g_i = \phi_i V_i c_i$, see (19). Thus, we can rewrite (24) as

$$\begin{aligned}\lambda\phi_i V_i c_i^*(\lambda) = \phi_i V_i c_i(t=0) + \sum_{[ik]} b_{ik} \frac{\lambda c_k^*(\lambda)}{\lambda + \alpha_k[1 - p_k^*(\lambda)]} \\ - \sum_{[ik]} b_{ik} \frac{\lambda c_i^*(\lambda)}{\lambda + \alpha_i[1 - p_i^*(\lambda)]}\end{aligned} \tag{26}$$

As in the previous, we obtain in the limit $\xi_{ij} \to 0$ the spatially continuous equation

$$\phi(\mathbf{x})\lambda c^*(\mathbf{x},\lambda) - \nabla \cdot D(\mathbf{x})\nabla\mu^*(\mathbf{x},\lambda)c^*(\mathbf{x},\lambda) = \phi(\mathbf{x})c(\mathbf{x},t=0), \tag{27}$$

in which we defined the memory function

$$\mu^*(\mathbf{x},\lambda) = \frac{\lambda}{\lambda + \alpha(\mathbf{x})[1-p^*(\mathbf{x},\lambda)]}. \tag{28}$$

In real time, we obtain from (27) by inverse Laplace transform the non-local heterogeneous diffusion problem

$$\phi(\mathbf{x})\frac{\partial c(\mathbf{x},t)}{\partial t} = \nabla \cdot D(\mathbf{x})\nabla \int_0^t dt' c(\mathbf{x},t')\mu(\mathbf{x},t-t'). \tag{29}$$

This equation models heterogeneous diffusion together with heterogeneous multirate mass transfer. In this context, the mobile solute concentration $c_m(\mathbf{x},t)$ is defined as [34]

$$c_m(\mathbf{x},t) = \int_0^t dt' c(\mathbf{x},t')\mu(\mathbf{x},t-t'). \tag{30}$$

The porosity $\phi(\mathbf{x})$ now is divided into the mobile and immobile porosities, $\phi_m(\mathbf{x})$ and $\phi_{im}(\mathbf{x})$, respectively, such that $\phi(\mathbf{x})c(\mathbf{x},t) = \phi_m(\mathbf{x})c_m(\mathbf{x},t) + \phi_{im}(\mathbf{x})c_{im}(\mathbf{x},t)$. The immobile concentration is denoted by $c_{im}(\mathbf{x},t)$. We consider a scenario for which the solute is initially distributed in the mobile domain. Thus, by inserting the Laplace transform of (30) into (27) gives for the mobile concentration

$$\frac{\phi(\mathbf{x})}{\mu^*(\mathbf{x},\lambda)}\lambda c_m^*(\mathbf{x},\lambda) - \nabla \cdot D(\mathbf{x})\nabla c_m^*(\mathbf{x},\lambda) = \phi_m(\mathbf{x})c_m(\mathbf{x},t=0), \tag{31}$$

where the right side reflects the fact that initially there is only solute in the mobile domain. We now establish the relation between the memory function $\mu(\mathbf{x}, t)$ and the transfer function $\varphi(\mathbf{x}, t)$ given within the context of MRMT. The MRMT approach gives the following non-local transport equation for the mobile concentration [e.g., 33, 38]

$$\phi_m(\mathbf{x})\frac{\partial c_m(\mathbf{x},t)}{\partial t} + \phi_{im}(\mathbf{x})\frac{\partial}{\partial t}\int_0^t dt'\varphi(\mathbf{x},t-t')c_m(\mathbf{x},t') = \nabla\cdot D(\mathbf{x})\nabla c_m(\mathbf{x},t). \tag{32}$$

The difference to the formulations given in Refs. [33, 38] are due to the non-zero initial condition employed here. The site-dependent transfer function $\varphi(\mathbf{x}, t)$ encodes the details of the microscopic mass transfer mechanisms between the mobile and immobile regions [e.g., 39, 34]. Comparing the Laplace transform of (32) with (31) gives the following relation between the memory function $\mu^*(\mathbf{x}, \lambda)$ and the transfer function $\varphi^*(\mathbf{x}, \lambda)$

$$\mu^*(\mathbf{x},\lambda) = \frac{\phi(\mathbf{x})}{\phi_m(\mathbf{x}) + \phi_{im}(\mathbf{x})\varphi^*(\mathbf{x},\lambda)}. \tag{33}$$

For the relation between the Laplace transforms of the transfer function, $\varphi^*(\mathbf{x}, \lambda)$, and the trapping time distribution, $p^*(\mathbf{x}, \lambda)$, we obtain by using (28)

$$\varphi^*(\mathbf{x},\lambda) = \frac{\phi(\mathbf{x})}{\phi_{im}(\mathbf{x})} - \frac{\phi_m(\mathbf{x})}{\phi_{im}(\mathbf{x})} + \frac{\alpha(\mathbf{x})\phi(\mathbf{x})}{\phi_{im}(\mathbf{x})\lambda}\left[1 - p^*(\mathbf{x},\lambda)\right]. \tag{34}$$

3. Model Setup and Numerical Implementation

We consider diffusion in the d-dimensional domain Ω with the $(d-1)$-dimensional boundaries B_Ω. In the following we use regular meshes in $d = 2$ and $d = 1$ spatial dimensions. Consequently the internodal distance is $\xi_{ij} = \xi$

is constant. Thus, the interfacial area S_{ij} between the pixels i and j is constant and given by $S = \xi^{d-1}$ and so is the volume of the pixel, $V_i = V = \xi^d$. The normalized transition probability w_{ij} from position j to position i is given by (18).

No flow boundary conditions are treated as a zero diffusion limit ($w_{ij} = 0$). Dirichlet boundary conditions at the inlet $B_\Omega^{in} \subset B_\Omega$ (constant concentration) are implemented as described in the following. The inlet B_Ω^{in} is formed by P_{in} pixels. At each of these pixels the concentration is constant, $c_i = c^{in}$ for $i = 1, \ldots, P_{in}$. Note that for $d = 1$ spatial dimension $P_{in} = 1$. In the numerical particle tracking simulations, however, we do not prescribe the concentration at the inlet boundary, but the number of particles at each node. Therefore, we consider the number density g_i given by (19). Its values at the boundary nodes is given by $g_i^{in} = \phi_i V c^{in}$. Since the g_i are in general not normalized, we define now the normalized number density as

$$n_i = \frac{g_i}{\sum_{j=1}^{P_{in}} g_j^{in}} = \frac{\phi_i c_i}{c^{in} \sum_{j=1}^{P_{in}} \phi_j}. \tag{35}$$

This is the observable that we obtain from the TDRW simulations, namely n_i is equal to the number N_i of particles in the pixel normalized by the number of particles N on the boundary, $n_i = N_i/N$. Thus, the concentration c_i at pixel i is given in terms of the n_i as

$$c_i = n_i \frac{c^{in} \sum_{j=1}^{P_{in}} \phi_j}{\phi_i}. \tag{36}$$

The number N_i^{in} of particles at the boundary pixels then are given by

$$N_i^{in} = N \frac{\phi_i}{\sum_{j=1}^{P_{in}} \phi_j} \tag{37}$$

for $i = 1, \ldots, P_{in}$.

An absorbing boundary condition (zero concentration) at the outlet boundary $B_\Omega^{out} \subset \Omega$ is implemented by removing particles as they cross B_Ω^{out}. The outlet boundary is formed by P_{out} pixels. Note that $P_{out} = 1$ in $d = 1$ spatial dimension. The cumulative distribution of arrival times $F(t)$ at the outlet boundary then is given by

$$F(t) = \frac{1}{N} \sum_{j=1}^{P_{out}} N_j(t), \tag{38}$$

where $N_j(t)$ is the number of particles that have crossed the outlet boundary until time t. Correspondingly, the distribution density of arrival times, $f(t)$, is

$$f(t) = \frac{1}{N} \sum_{j=1}^{P_{out}} \frac{\Delta N_j(t)}{\Delta t}, \tag{39}$$

where $\Delta N_j(t)$ is the number of particles that crosses the outlet during the sampling interval $[t, t + \Delta t]$.

3.1. Interpixel Diffusion Coefficients

In Section 2.2, we left intentionally open how to choose the interpixel diffusion coefficients $\hat{D}_{ij}$. Frequently, it is determined as the harmonic average between the diffusion coefficient in adjacent pixels [e.g., 4]. Here we want to compare the performance of different choices for the interpixel diffusion coefficient.

To this end, we consider diffusion in a two-dimensional domain of length $L = 10^2\xi$ and width $d = 50\xi$. It is characterized by a spatially varying diffusion coefficient $D(\mathbf{x})$ and constant porosity $\phi(\mathbf{x}) = \phi = 1$. The heterogeneous

domain is generated by assigning to each pixel in the domain randomly diffusion coefficients that are chosen independently, from a lognormal distribution characterized by the geometric average $D_G = 0.5$ and variance of $\ln D$ given by $\sigma^2_{\ln D} = 1$. We record the vertically averaged concentration close to the outlet at $x_1 = 90\xi$ and compare it to the analytical solution for the equivalent homogeneous problem. Specifically, we consider the case of an instantaneous solute pulse at the inlet boundary at $x_1 = 0$. The position vector here is $\mathbf{x} = (x_1, x_2)^T$.

It was shown by Matheron [40] that the exact effective diffusion coefficient D^e for this setup is given by the geometric mean $D^e = D_G$ of the lognormally distributed $D(\mathbf{x})$. Thus, the equivalent homogeneous diffusion problem for $c(x_1, t) = d^{-1} \int_0^d dx_2 c(\mathbf{x}, t)$ is one-dimensional and characterized by the geometric mean diffusion coefficient D_G,

$$\frac{\partial c(x_1, t)}{\partial t} - D_G \frac{\partial^2 c(x_1, t)}{\partial x_1^2} = 0, \tag{40}$$

with the initial condition $c(x_1, t = 0) = 0$. The boundary condition at the outlet is $c(L, t) = 0$, the one at the inlet is $c(0, t) = j_0 \delta(t)$. The solute flux j_0 is given by $j_0 = c_0 \tau_p$ with c_0 the concentration on the inlet boundary and τ_p the pulse duration. The analytical solution for $c(x_1, t)$ then is given by [e.g., 41]

$$c(x_1, t) = j_0 \frac{2 D_G \pi}{L^2} \sum_{n=1}^{\infty} n \sin\left(\frac{n \pi x_1}{L}\right) \exp\left(-\frac{n^2 D_G \pi^2 t}{L^2}\right), \tag{41}$$

In the following $d = 2$ dimensional numerical simulations, we apply the concentration $c_0 = 1/\xi^2$. The pulse duration τ_p is given by the mean diffusion time over one pixel $\tau_p = \xi^2/(2D_G)$. Thus, we have $j_0 = 1/(2D_G)$. At the

horizontal boundaries at $x_2 = 0$ and $x_2 = d$ no-flux boundary conditions are specified. The domain size is $L = 10$ m.

We compare this analytical solution for the exact average diffusion problem (40) to the outcome of the corresponding TDRW simulations for two difference choices of the interpixel diffusion coefficient, namely (i) the harmonic mean and (ii) the geometric mean of the diffusion coefficients in adjacent pixels. The choice that yields the best comparison with the exact average solution will be employed in the following numerical simulations.

Figure B.2 displays the vertically averaged and normalized concentration $c_L(t)$ close to the outlet boundary at $L = 90\xi$ obtained from the TDRW simulation for the two different interpixel diffusion coefficients. It is compared to $c(x_1, t)$ for the equivalent homogeneous medium given by (41) with $D_G = 0.52$. We observe that the interpixel diffusion coefficient given by the geometric mean gives the best agreement with the analytical solution. Therefore, in the following $d = 2$ dimensional TDRW simulations we will employ the geometric mean for the interpixel diffusion coefficients

$$\hat{D}_{ij} = \sqrt{D_i D_j}. \tag{42}$$

Note that it is beyond the scope of the present paper to demonstrate that it is the best approximation for non-lognormal distributions or for three-dimensional transport. This issue is in fact not specific to the TDRW approach but concerns all discretized methods applied to heterogeneous diffusion problems.

For the $d = 1$ dimensional TDRW simulations presented in the following,

the interpixel diffusion coefficient is given by the harmonic mean

$$\hat{D}_{ij} = D_H = 2\frac{D_i D_j}{D_i + D_j}. \tag{43}$$

The pulse duration τ_p is as above given by the mean diffusion time over one pixel $\tau_p = \xi^2/(2D_H)$, the boundary concentration, however, is $c_0 = 1/\xi$. Thus, for $d = 1$we have $j_0 = \xi/(2D_H)$.

Also note that the setup considered here corresponds to a pulsed through diffusion test. Diffusion experiments (or through diffusion tests) are widely used for measuring the effective diffusion of low permeability porous media, such as manufactured cements or consolidated argillaceous formations considered as potential host rock for radioactive waste repositories [42]. At the laboratory scale such experiments consist in applying a constant concentration gradient across a thin core of rock by maintaining constant concentration at the two edges (usually a zero concentration at the outlet) and recording the solute flux at the outlet [10].

3.2. Heterogeneous Diffusion

The heterogeneous diffusion problem (1) is solved using the random walk particle tracking scheme (4) with the transition time density (13) and the transition probabilities w_{ij} and the mean transition time τ_j given by (21). The transport time is updated for each particle transition according to

$$t_{n+1} = t_n + \theta_j, \qquad \theta_j = -\tau_j \ln(\eta_n), \tag{44}$$

where the random variable η_n is uniformly distributed in $[0, 1]$.

3.3. Diffusion with Multirate Mass Transfer

In Section 2.3, we showed that MRMT can be modeled in the TDRW context by introducing particle traps characterized by a given distribution of trapping times. The resulting TDRW-MRMT model is implemented following Ref. [35]. First, we note that the transition time θ_j, which is distributed according to (13), measures the total time the particle is mobile. During this mobile time, the particle can get trapped at the constant rate α_j, see Section 2.3. The times the particle are mobile between trapping events is denoted by $\hat{\theta}_j$. Since trapping occurs at constant rate, $\hat{\theta}_j$ is exponentially distributed

$$p_{mj}(t) = \alpha_j \exp(-\alpha_j t). \tag{45}$$

The number of trapping events that actually occur during a mobile transition of time θ_j, n_{θ_j}, is the random number that fulfills

$$n_{\theta_j} = \max\left(n \left| \sum_{l=1}^{n} \hat{\theta}_{jl} \leq \theta_j < \sum_{l=1}^{n+1} \hat{\theta}_{jl} \right. \right). \tag{46}$$

It is a renewal process, and specifically, for the exponential distribution (45), it is a Poisson process. The distribution $p_n(n|\theta_j)$ of n_{θ_j} thus is given by the Poisson distribution

$$p_n(n|\theta_j) = \frac{(\alpha_j \theta_j)^n}{n!} \exp(-\alpha_j \theta_j). \tag{47}$$

The unconditional distribution of the number of trapping events at pixel j then is given by

$$p_{n_j}(n) = \int_0^\infty dt \psi_j(t) p_n(n|t) = \frac{n(\alpha_j \tau_j)^n}{(\alpha_j \tau_j + 1)^{n+1}}, \tag{48}$$

in which we used (13) for $\psi_j(t)$. Thus, the mean number of trapping events $\overline{n}_j$ at pixel j is given by $\overline{n}_j = \alpha_j \tau_j$. The overbar in the following denotes the noise average over all particles. The spatial average of the mean numbers of trapping events per pixel is $N_{\text{trap}} = \langle \overline{n}_j \rangle$. The spatial average over all pixels is denoted by angular brackets.

In general, the trapping rate α_j is spatially distributed and can be considered as a property of the heterogeneous medium. For the following analysis, we correlate the trapping rate to porosity and assume that the noise mean number of traps at pixel j is inversely proportional to porosity, $\overline{n}_j = A\phi_j^{-1}$ with A a constant of proportionality. This relates the trapping rate α_j to porosity as $\alpha_j = A/(\phi_j \tau_j)$. Note also that the spatial average number of trapping events under this assumption is given by $N_{\text{trap}} = A/\phi_H$, where ϕ_H is the harmonic mean of porosity over all locations. Thus, we can express the proportionality constant A in terms of the average number of traps per pixel, N_{trap}, as $A = N_{\text{trap}}\phi_H$ and therefore set

$$\alpha_j = \frac{N_{\text{trap}}\phi_H}{\tau_j \phi_j}, \qquad\qquad \overline{n}_j = N_{\text{trap}} \frac{\phi_H}{\phi_j}. \tag{49}$$

We now can determine the total transition time, denoted by Θ_j. It is given by the sum of the total mobile time θ_j at pixel j and the sum over the trapping times, denoted here by ϑ_j,

$$\Theta_j = \theta_j + \sum_{l=1}^{n_{\theta_j}} \vartheta_{jl}, \tag{50}$$

where n_{θ_j} is given by (46). Note that the sum on the right hand side denotes a compound Poisson process. Time now is updated by

$$t_{n+1} = t_n + \Theta_j. \tag{51}$$

4. Numerical Simulations

As mentioned in the Introduction, there are many processes driven by diffusive transport in media displaying heterogeneous diffusion properties. Here, we focus on the diffusion of solute in porous media. Furthermore, in the following we will assume for simplicity that $D(\mathbf{x}) = \phi(\mathbf{x})D_0$ where D_0 is the coefficient for free diffusion in water. More general formulations such as $D(\mathbf{x}) = \phi(\mathbf{x})^n D_0$ as proposed by [5] can be implemented easily, as well as the assumption that $\phi(\mathbf{x})$ and $D(\mathbf{x})$ are independent.

4.1. Heterogeneous Diffusion in Porous Media

We consider a scenario which corresponds to a pulse diffusion test which allows to deduce the distribution of residence times in a heterogeneous rock sample.

The transfer function $\varphi(t)$ for a low permeability rock sample is of central concern for transport modeling in the framework of multirate mass transfer, see Section 2.3. It is related to the distribution of residence times $p(t)$ through expression (34). For purely diffusive mass transfer between a mobile region and immobile regions, which in general is characterized by heterogeneous diffusion properties, the transfer function $\varphi(t)$ encodes the fraction of rock matrix containing connected micro-porosity or inter-grain porosity as well as stagnant and trapped water [5]. The transfer function integrates, by definition, all the information on the geometry and the heterogeneous diffusion properties of the immobile domain as well as its accessibility to tracer particles from the mobile domain (this means, the properties of the mobile-immobile interfacial area). Therefore, for a given value of D_0, the

memory function can be considered as an intrinsic property of the rock characterizing its immobile fraction. Gouze et al. [5] showed that the parameters necessary for characterizing diffusion in the 3D immobile domain, i.e., mainly the porosity distribution and the boundary geometry, can be extracted from X-ray microtomography.

By definition, the transfer function is related to the probability that a tracer particle entering the immobile zone at $t = 0$ remains in it until time t [43], see also (34). Consequently, computing the memory function with the TDRW method consists in applying an instantaneous solute pulse at the mobile-immobile interface and record the residence time of the particles that enter the immobile domain. As the immobile domain geometry is very complex (both in terms of boundary conditions and diffusion coefficient variability within the immobile domain) computations in $d = 3$ spatial dimensions for pertinent representative elementary volumes (order of 10^6 voxels) are usually prohibitive using standard random walk methods with constant time increments. The TDRW method provides an efficient alternative.

Two examples of computed memory functions are given in Figure B.3. The first one concerns the memory function of a sphere of constant porosity for which the analytical solution is known [33]. In this case we obtain a memory function characterized by a power-law tail $\varphi(t) \propto t^{-\beta}$ with exponent $\beta = 1/2$. The second example calculates the memory function for a natural rock sample (limestone). Figure B.3 illustrates the long-time tail of $\varphi(t)$ associated with the natural rock denoting the strong retention of the particles in the immobile domain triggered by the tortuosity and the variability of the diffusion paths. In this case we obtain a memory function with exponent

$\beta = 1.1$.

4.2. Diffusion with Multirate Mass Transfer

Here we consider the diffusion model combined with multirate mass transfer as described in Sections 2.3 and 3.3. For computational simplicity, we consider a $d = 1$ dimensional setup. In the absence of traps, diffusion is described by

$$\phi(x)\frac{\partial c(x,t)}{\partial t} - \frac{\partial}{\partial x}\phi(x)D_0\frac{\partial}{\partial x}c(x,t) = 0. \tag{52}$$

The equivalent homogeneous model is given by

$$\phi_A\frac{\partial \overline{c}(x,t)}{\partial t} - \frac{\partial}{\partial x}\phi_H D_0\frac{\partial}{\partial x}\overline{c}(x,t) = 0, \tag{53}$$

see Appendix A.

The domain is initially solute free. We consider as boundary conditions a solute pulse at the inlet, $c(0,t) = j_0\delta(t)$, and zero concentration at the outlet at $x = L$, $c(L,t) = 0$.

The heterogeneous diffusion problem (52) is non-dimensionalized by setting $x = \tilde{x}L$, $t = \tilde{t}\tau_L$ and $c(x,t) = \tilde{c}(x/L, t/\tau_L)j_0/\tau_L$, where $\tau_L = L^2/D_0$. Thus, we obtain from (52)

$$\phi(\tilde{x})\frac{\partial \tilde{c}(\tilde{x},\tilde{t})}{\partial \tilde{t}} - \frac{\partial}{\partial \tilde{x}}\phi(\tilde{x})\frac{\partial}{\partial \tilde{x}}\tilde{c}(\tilde{x},\tilde{t}) = 0. \tag{54}$$

The non-dimensional inlet boundary condition is given by $\tilde{c}(\tilde{x} = 0, \tilde{t}) = \delta(\tilde{t})$. In the following, all quantities are non-dimensional, the tildes are omitted for simplicity of notation.

The mass transfer properties in the following are assumed to be uniform, that is, the trapping time ϑ_j is independent of the pixel position, $\vartheta_j = \vartheta$,

and therefore $p_j(t) = p(t)$. For illustration, we consider a (truncated) Pareto distribution for the trapping times, which can account for the occurrence of a broad distribution of heterogeneity length scales,

$$p(t) = \frac{\beta}{t_1[1-(t_1/t_2)^\beta]} \left(\frac{t}{t_1}\right)^{-1-\beta}, \qquad t_1 < t < t_2. \tag{55}$$

The median time scale t_1 is related to the smallest, the cut-off time t_2 to the largest heterogeneity feature. For this $d = 1$ dimensional scenario the transport equation (29) simplifies to

$$\phi(x)\frac{\partial c(x,t)}{\partial t} = \frac{\partial}{\partial x}\phi(x)\frac{\partial}{\partial x}\int_0^t dt' c(x,t')\mu(x,t-t'), \tag{56}$$

where the memory function $\mu(x,t)$ is given in Laplace space by, see (28),

$$\mu^*(x,\lambda) = \frac{\lambda}{\lambda + \alpha(x)[1-p^*(\lambda)]}. \tag{57}$$

The trapping rate $\alpha(x)$ depends on porosity as given by (49).

For the numerical simulations presented in the following, the domain is discretized into 10^2 pixels. For the simulations of heterogeneous diffusion, porosity values are assigned randomly to each pixel according to a truncated Gaussian distribution,

$$p_\phi(f) = A_\phi^{-1}\Theta(f-\phi_b)\Theta(\phi_t - f)\frac{\exp\left[-\frac{(f-\phi_A)}{2\sigma_\phi^2}\right]}{\sqrt{2\pi\sigma_\phi^2}}, \tag{58}$$

in which the normalization constant A_ϕ is given by

$$A_\phi = \int_{\phi_b}^{\phi_t} df \frac{\exp\left[-\frac{(f-\phi_A)}{2\sigma_\phi^2}\right]}{\sqrt{2\pi\sigma_\phi^2}}. \tag{59}$$

The lower cut-off of the porosity distribution is set to $\phi_b = 0.2$, the upper cut-off to $\phi_t = 0.8$. The standard deviation is set to $\sigma_\phi = 0.2$. The median time scale t_1 in (55) is set to $t_1 = 2.5 \times 10^{-3}$.

Figure (B.4) illustrates the evolution of concentration at $x_1 = 0.1$, $x_2 = 0.5$ and $x_3 = 0.9$ for the heterogeneous model without traps and the equivalent homogeneous model, which is characterized by the arithmetic and harmonic averages of the porosity values within the domain, see (53) and Appendix A. Close to the inlet boundary at x_1, we observe an intermediate time regime characterized by a power-law $c(x_1, t) \propto t^{-\gamma}$ with exponent $\gamma = 3/2$. This behavior is characteristic for diffusion in a homogeneous semi-infinite medium, which is a valid approximation far away from the outlet boundary. In fact, in the time regime $x^2 \ll t \ll 1$, the solution of (53) can be approximated by (see Appendix B)

$$c(x,t) = \frac{x \exp\left(-\frac{x^2 \phi_A}{4\phi_H t}\right)}{\sqrt{4\pi\phi_A/\phi_H} t^{-3/2}}, \tag{60}$$

which gives the observed $t^{-3/2}$ behavior. The characteristic power-law can only be observed in the intermediate regime $x^2 \ll t \ll 1$. The lower bound denotes the typical non-dimensional diffusion time to arrive at x, while the upper bound, 1, is the non-dimensional diffusion time to the outlet boundary. Thus, at times larger than 1 particles leave the system at the absorbing boundary at $x = 1$ and the approximation of a semi-infinite medium does not hold anymore. This explains the breakdown of the power-law behavior, that is the cut-off, at time 1. For x_1, this regime is well developed. For increasing x, this regime shrinks and no power-law behavior is observable.

Figure B.5 shows the evolution of the solute concentration $c(x_1, t)$ with

time at $x_1 = 0.1$, $x_2 = 0.2$ in the presence of traps ($N_{\text{Trap}} = 3$) with $\beta = 2/5$ in (55) and cut-off times of $t_2 = 1$, $t_2 = 10^3$, $t_2 = 10^7$, $t_2 = 10^{10}$ and $t_2 = \infty$. The peak times are shifted to significantly larger times compared to the case without traps. The time evolution of concentration is cut-off now at a scale t_c that is given by the trapping rate α, (49), and the mean trapping time $\bar{t}$, $t_c \approx \alpha\bar{t}$. The trapping rate α here is of the order of 10^4. This behavior is discussed in Appendix B for an equivalent homogeneous case. For $t_2 = 1$, the mean trapping time $\bar{t} \approx 0.4$, and thus the cut-off time is of the order of $t_c \approx 10^3$. The cutoff time t_2 here is much smaller than t_c, $t_2 \ll t_c$. Thus, we can still observe the characteristic $t^{-3/2}$ behavior in the time regime $t_2 \ll t \ll t_c$ because in this regime, concentration behaves essentially like in the case without traps, but characterized by a renormalized diffusion coefficient, see Appendix B.

As t_2 increases, this behavior changes. The peak of $c(x,t)$ becomes wider and $c(x,t)$ decreases with a flatter slope. As long as the cut-off time is smaller than t_c, the evolution of $c(x,t)$ is essentially truncated at t_c.

In the case of a pure power-law, that is $t_2 = \infty$, a persistent power-law regime develops at asymptotically long times for $t \gg t_1\alpha^{1/\beta}$, where α is the trapping rate, see Appendix B. In this regime $c(x,t)$ behaves as $c(x,t) \propto t^{-\beta}$.

In the case of a finite truncation time t_2, an intermediate power-law regime develops if $t_2 \gg t_1\alpha^{1/\beta} \gg t_1$. For this scale order the power-law behavior $c(x,t) \propto t^{-\beta}$ can be observed in the regime $t_1\alpha^{1/\beta} \ll t \ll t_2$. Concentration $c(x,t)$ is then truncated at the cut-off scale t_2. These behaviors are discussed in more detail for an equivalent homogeneous medium in Appendix B.

5. Summary and Conclusions

TDRW is a computationally robust and efficient method to model diffusion in discretized heterogeneous media. It is specifically adapted to perform calculations on constant-size voxelized media such as 3D porosity images obtained by processing X-ray microtomography. The efficiency of the method is due to its intrinsic compliance with parallel computing and the few calculations required. Accordingly, TDRW has often been used for diffusion calculations during the last decade, replacing standard methods, such as finite differences, finite elements or random walk method based on constant time discretization. Nevertheless, to the best of our knowledge, its equivalence with spatially discretized heterogeneous diffusion equation has not been formally proved, albeit its ability to reproduce analytical solution for homogeneous cases has been broadly verified.

In this paper we demonstrated that the TDRW scheme, that is, the CTRW (4) characterized by the exponential transition time density (13) and the transition probabilities and mean transition times (21), is equivalent to the finite volume discretization of the heterogeneous diffusion equation (1). Based on this insight, we developed a TDRW particle scheme that models multiple trapping events (TDRW-MRMT), which can account for linear kinetic sorption-desorption reactions and solute trapping due to unresolved subscale heterogeneities. We provide an exact numerical algorithm for the implementation of the TDRW-MRMT based on CTRW theory. The TDRW approach is illustrated for the calculation of the residence time distribution in heterogeneous rocks. The TDRW-MRMT method is used to study diffusion in a bounded $d = 1$ dimensional medium in the presence of traps character-

ized by a truncated power-law trapping time distribution. We identify time regimes of anomalous behavior and discuss the truncation time of the evolution of the concentration distribution at an observation point in function of the cut-off time scale of the truncation power-law.

In summary, the presented developments provide a solid theoretical basis of the TDRW method and a novel TDRW-MRMT framework to account for the impact of subscale heterogeneities on diffusion behavior in heterogeneous media.

Acknowledgements: The support through the European Union project MUSTANG (UE-7thFP-ENERGY 227286) and the French National Research Agency (project CO-LINER, ANR-08-PCO2- 004-01) is gratefully acknowledged.

Appendix A. Equivalent Homogeneous Model

We seek the equivalent homogeneous model for the heterogeneous diffusion equation (52). The homogeneous model is defined as

$$\phi^e \frac{\partial \overline{c}(x,t)}{\partial t} - D^e \frac{\partial^2 \overline{c}(x,t)}{\partial x^2} = 0, \tag{A.1}$$

with the effective porosity ϕ^e and effective diffusivity D^e. The aim is to determine these effective porosities. To this end, we consider the following criteria. The effective model (A.1) should reproduce the correct average steady state concentrations and solute fluxes. The steady state concentration $c_s(x) = \lim_{t\to\infty} c(x,t)$ satisfies

$$\frac{\partial}{\partial x}\phi(x) D_0 \frac{\partial}{\partial x} c_s(x) = 0. \tag{A.2}$$

For the first criterion we consider a situation with no flux boundary conditions in a bounded domain. The solution is $c_s(x) = c_0 = \text{constant}$. Thus, we obtain in equilibrium for the average bulk concentration $g(x,t) = \phi(x)c(x,t)$

$$\overline{g_s(x)} = \overline{\phi(x)c_s(x)} = \overline{\phi(x)}c_0. \tag{A.3}$$

The effective porosity ϕ^e is equal to the arithmetic average porosity $\phi^e = \phi_A$.

The second criterion refers to the average flux. We consider a scenario characterized by unit concentration at the inlet at $x = 0$ and zero concentration at the outlet at $x = L$. The solution for the concentration distribution then is given by

$$c_s(x) = -\frac{\phi_H}{L}\int_0^x \frac{dx'}{\phi(x)} \tag{A.4}$$

with ϕ_H the harmonic average porosity. Thus, the average solute flux is given by

$$\overline{\phi(x)D_0\frac{\partial c_s(x)}{\partial x}} = \phi_H D_0 \frac{\partial \overline{c}_s(x)}{\partial x}. \tag{A.5}$$

This result is of course well known. The effective diffusivity D^e in the flux term is given by $D^e = \phi_H D_0$.

Appendix B. Diffusion and Multitrapping in Finite Domain

The solution for the diffusion problem (53) in Laplace space is given by

$$c^*(x,\lambda) = \frac{\sinh\left[(1-x)\sqrt{\frac{\lambda\phi_A}{\phi_H}}\right]}{\sinh\left(\sqrt{\frac{\lambda\phi_A}{\phi_H}}\right)}. \tag{B.1}$$

This can be checked by inspection. At times small compared to the dimensionless diffusion scale, which here is equal to 1, this means for $\lambda \gg 1$, this expression can be approximated by

$$c^*(x,\lambda) = \exp\left(-x\sqrt{\frac{\lambda\phi_A}{\phi_H}}\right). \tag{B.2}$$

The solution for $c(x,t)$ is then given by inverse Laplace transform and yields (60).

We now consider the equivalent case of homogeneous diffusion with multirate mass transfer. For simplicity we set here $\phi_A = \phi_H$ (note that for the parameter values used for the simulations in Section 4.2, $\phi_A \approx \phi_H$)

$$\frac{\partial c(x,t)}{\partial t} = \frac{\partial^2}{\partial x^2}\int_0^t dt' c(x,t')\mu(t-t'). \tag{B.3}$$

The memory function (57) is independent of space. Note that $c(x,t)$ denotes the total solute concentration, the injection, however, is with respect to the mobile solute only. Thus, by virtue of (30), the boundary condition for $c(x,t)$ is expressed as

$$\int_0^t dt' c(x=0,t')\mu(0,t-t') = \delta(t). \tag{B.4}$$

The solution of (B.3) in Laplace space is given by

$$c^*(x,\lambda) = \frac{\sinh\left[(1-x)\sqrt{\frac{\lambda}{\mu^*(\lambda)}}\right]}{\mu^*(\lambda)\sinh\left[\sqrt{\frac{\lambda}{\mu^*(\lambda)}}\right]}. \tag{B.5}$$

Inserting expression (57) for $\mu^*(\lambda)$ gives the Laplace transform of concentration in function of $p^*(\lambda)$

$$c^*(\tilde{x},\lambda) = \frac{\lambda+\alpha[1-p^*(\lambda)]}{\lambda}\frac{\sinh\left\{(1-x)\sqrt{\lambda+\alpha[1-p^*(\lambda)]}\right\}}{\sinh\left\{\sqrt{\lambda+\alpha[1-p^*(\lambda)]}\right\}}. \tag{B.6}$$

In order to analyze the behaviors and regimes, we need to determine the behavior of $p^*(\lambda)$. For this purpose, we consider the Laplace transform of the truncated power-law (55), which is given by

$$p^*(\lambda) = \frac{1}{1-(t_1/t_2)^\beta}\left[\exp(-\lambda t_1) - (t_1/t_2)^\beta \exp(-\lambda t_2)\right] + \frac{(\lambda t_1)^\beta}{1-(t_1/t_2)^\beta}\left[\Gamma(1-\beta,\lambda t_1) - \Gamma(1-\beta,\lambda t_2)\right], \tag{B.7}$$

where $\Gamma(\alpha, x)$ is the incomplete Gamma function [30]. Note that here $0 < \beta < 1$. For times larger than the cut-off time t_2, which corresponds to $\lambda \ll t_2^{-1}$, this expression can be approximated by

$$p^*(\lambda) \approx 1 - \bar{t}\lambda, \qquad \bar{t} = t_1 \frac{\beta}{1-\beta}\frac{(t_2/t_1)^{1-\beta}-1}{1-(t_1/t_2)^\beta}. \tag{B.8}$$

Note that $\bar{t}$ is the mean trapping time. Inserting the latter into (B.6) gives

$$c^*(\tilde{x},\lambda) = (1+\alpha\bar{t})\frac{\sinh\left[(1-x)\sqrt{\lambda(1+\alpha\bar{t})}\right]}{\sinh\left[\sqrt{\lambda(1+\alpha\bar{t})}\right]}. \tag{B.9}$$

Let us consider now the λ range for which the argument of the hyperbolic sine is small compared to 1. This is the case for $\lambda \ll (1+\alpha\bar{t})$, which gives in time, $t \gg (1+\alpha\bar{t}) = t_c$. The scale t_c is essentially given by the trapping rate α and the mean trapping time. This scale corresponds to the time at which concentration is cut-off. Specifically, if the cutoff time t_2 is much smaller than t_c, $t_2 \ll t_c$, we observe the characteristic $t^{-3/2}$ behavior in the time regime $t_2 \ll t \ll t_c$ because in this regime, concentration behaves as in the case without traps, but characterized by a renormalized diffusion coefficient.

In the time regime $t_1 \ll t \ll t_2$, (B.8) can be approximated by

$$p^*(\lambda) \approx 1 - a_\beta \lambda^\beta, \qquad a_\beta = t_1^\beta \Gamma(1-\beta) \tag{B.10}$$

Inserting the latter into (B.6), gives

$$c^*(x,\lambda) = (1+\alpha a_\beta \lambda^{\beta-1}) \frac{\sinh\left[(1-x)\sqrt{\lambda+\alpha a_\beta \lambda^\beta}\right]}{\sinh\left[\sqrt{\lambda+\alpha a_\beta \lambda^\beta}\right]}. \tag{B.11}$$

For $\lambda \ll t_1^{-1}[\alpha\Gamma(1-\beta)]^{-\frac{1}{\beta}}$, this means, if the argument of the hyperbolic sine is small, this expression can be approximated as

$$c^*(x,\lambda) \approx \alpha a_\beta \lambda^{\beta-1}, \tag{B.12}$$

which yields the power-law behavior

$$c(x,\lambda) \propto t^{-\beta} \tag{B.13}$$

for times $t \gg t_1[\alpha\Gamma(1-\beta)]^{\frac{1}{\beta}}$. Note, however, that this power-law behavior can only be observed if the cut-off scale t_2 is larger than $t_1[\alpha\Gamma(1-\beta)]^{\frac{1}{\beta}}$. In this case, one obtains the intermediate power-law time regime $t_1[\alpha\Gamma(1-\beta)]^{\frac{1}{\beta}} \ll t \ll t_2$.

[1] J. W. Haus, K. W. Kehr, Diffusion in regular and disordered lattices, Phys. Rep. 150 (1987) 263–406.

[2] S. Havlin, D. Ben-Avraham, Diffusion in disordered media, Adv. Phys. 51 (2002) 187–292.

[3] D. S. Dean, I. T. Drummond, R. R. Horgan, Effective transport properties for diffusion in random media, J. Stat. Mech. (2007) P07013.

[4] F. Delay, G. Porel, P. Sardini, Modelling diffusion in a heterogeneous rock matrix with a time-domain Lagrangian method and an inversion procedure, C. R. Geoscience 334 (2002) 967–973.

[5] P. Gouze, Z. Melean, T. Le Borgne, M. Dentz, J. Carrera, Non-fickian dispersion in porous media explained by heterogeneous microscale matrix diffusion, Water Resour. Res. 44 (2008) W11416.

[6] P. R. King, The use of field theoretic methods for the study of flow in a heterogeneous porous medium, J. Phys. A: Math. Gen. 20 (1987) 3935–3947.

[7] I. T. Drummond, R. R. Horgan, The effective permeability of a random medium, J. Phys. A: MAth. Gen. 20 (1987) 4661–4672.

[8] J. F. McCarthy, Continuous-time random walks on random media, J. Phys. A: Math. Gen. 26 (1993) 2495–2503.

[9] E. A. Codling, Random walk models in biology, J. R. Soc. Interface 5 (2008) 813–834.

[10] S. Pabitra, Time-dependent diffusion coefficient as a probe of geometry, Concepts in Magnetic Resonance Part A 23A (2004) 1–21.

[11] S. H. Patankar, Numerical Heat Transfer and Fluid Flow, Taylor and Francis, 1980.

[12] J. Crank, The Mathematics of Diffusion, Oxford University Press, 1975.

[13] W. Kinzelbach, The random walk method in pollutant transport simulation, in: E. Custodio (Ed.), Advances in analytical and numerical groundwater flow and quality modelling, Vol. 224 of C, NATO ASI, 1987, p. 227246.

[14] H. Risken, The Fokker-Planck Equation, Springer Heidelberg New York, 1996.

[15] S. C. James, C. V. Chrysikopoulos, An efficient particle tracking equation with a specified spatial step for the solution of the diffusion equation, Chem. Eng. Sci. 56 (2001) 65356543.

[16] F. Delay, P. Ackerer, C. Danquigny, Simulating solute transport in porous or fractured formations using random walk particle tracking: A review, Vadose Zone Journal 4 (2005) 360–379.

[17] O. Banton, F. Delay, G. Porel, A new time domain random walk method for solute transport in 1-D heterogeneous media, Ground Water 35 (1997) 1008–1013.

[18] B. Noetinger, T. Estebenet, Up-scaling of double porosity fractured media using continuous-time random walks methods, Transp. Porous Media 39 (2000) 315–337.

[19] P. W. Reimus, S. C. James, Determining the random time step in a constant spatial step particle tracking algorithm, Chem. Eng. Sci. 57 (2002) 4429–4434.

[20] F. Delay, J. Bodin, Time domain random walk method to simulate transport by advection-diffusion and matrix diffusion in fracture networks, Geophys. Res. Lett. 28 (2001) 4051–4054.

[21] J. Bodin, G. Porel, F. Delay, Simulation of solute transport in discrete fracture networks using the time domain random walk method, Earth Planet. Sci. Lett. 208 (2003) 297–304.

[22] E. W. Montroll, G. H. Weiss, Random walks on lattices, 2., J. Math. Phys. 6 (2) (1965) 167.

[23] H. Scher, M. Lax, Stochastic transport in a disordered solid. I. Theory, Phys. Rev. B 7 (1) (1973) 4491–4502.

[24] G. Zumofen, J. Klafter, Scale-invariant motion in intermittent chaotic systems, Phys. Rev. E 47 (1993) 851–863.

[25] B. Berkowitz, A. Cortis, M. Dentz, H. Scher, Modeling non-fickian transport in geological formations as a continuous time random walk, Rev. Geophys. 44 (2006) RG2003.

[26] B. Berkowitz, J. Klafter, R. Metzler, H. Scher, Physical pictures of transport in heterogeneous media: Advection-dispersion, random-walk, and fractional derivative formulations, Water Resour. Res. 38 (10) (2002) 1191. doi:10.1029/2001WR001030.

[27] I. Goychuk, Quantum dynamics with non-Markovian fluctuating parameters, Phys. Rev. E 70 (2004) 016109.

[28] A. V. Chechkin, R. Gorenflo, I. M. Sokolov, Fractional diffusion in inhomogeneous media, J. Phys. A 38 (2005) L679–L684.

[29] V. M. Kenkre, E. W. Montroll, M. F. Shlesinger, Generalized master equations for continuous-time random walks, J. Stat. Phys. 9 (1) (1973) 45–50.

[30] M. Abramowitz, I. A. Stegun, Handbook of Mathematical Functions, Dover Publications, New York, 1972.

[31] J. P. Bouchaud, A. Georges, Anomalous diffusion in disordered media: Statistical mechanisms, models and physical applications, Phys. Rep. 195 (4,5) (1990) 127–293.

[32] R. Haggerty, S. M. Gorelick, Multiple-rate mass transfer for modeling diffusion and surface reactions in media with pore-scale heterogeneity, Water Resour. Res. 31(10) (1995) 2383 2400.

[33] J. Carrera, X. Sanchez-Vila, I. Benet, A. Medina, G. Galarza, J. Guimera, On matrix diffusion, formulations, solutions methods and qualitative effects, Hydrogeol. J. 6(1) (1998) 178–190.

[34] M. Dentz, B. Berkowitz, Transport behavior of a passive solute in continuous time random walks and multirate mass transfer, Water Resour. Res. 39(5) (2003) 1111.

[35] D. A. Benson, M. M. Meerschaert, A simple and efficient random walk solution of multi-rate mobile/immobile mass transport equations, Adv. Water Resour. 32 (2009) 532–539.

[36] G. Margolin, M. Dentz, B. Berkowitz, Continuous time random walk and multirate mass transfer modeling of sorption, Chem. Phys. 295 (2003) 71–80.

[37] F. Delay, A. Kaczmaryk, P. Ackerer, Inversion of a Lagrangian time domain random walk (TDRW) approach to one-dimensional transport by derivation of the analytical sensitivities to parameters, Adv. Water Resour. 31 (2008) 484–502.

[38] R. Haggerty, S. A. McKenna, L. C. Meigs, On the late time behavior of tracer test breakthrough curves, Water Resour. Res. 36 (12) (2000) 3467—3479.

[39] C. F. Harvey, S. M. Gorelick, Temporal moment-generating equations: Modeling transport and mass transfer in heterogeneous aquifers, Water Resour. Res. 31 (8) (1995) 1895–1911.

[40] G. Matheron, Composition des perméabilités en milieu poreux, Revue de l'Institut Français du Petrole 23(2) (1968) 201–218.

[41] H. S. Carslaw, J. C. Jaeger, Conduction of Heat in Solids, Oxford University Press, 2008.

[42] C. Wittebroodt, S. Savoye, P. Gouze, Influence of initial iodide concentration on the iodide uptake by the Argillite of Tournemire, Physics and Chemistry of the Earth 33(14-16) (2008) 943–948.

[43] R. Haggerty, C. F. Harvey, C. Freiherr von Schwerin, L. C. Meigs, What controls the apparent timescale of solute mass transfer in aquifers and soils? A comparison of experimental results, Water Resour. Res. 40 (2004) W01510.

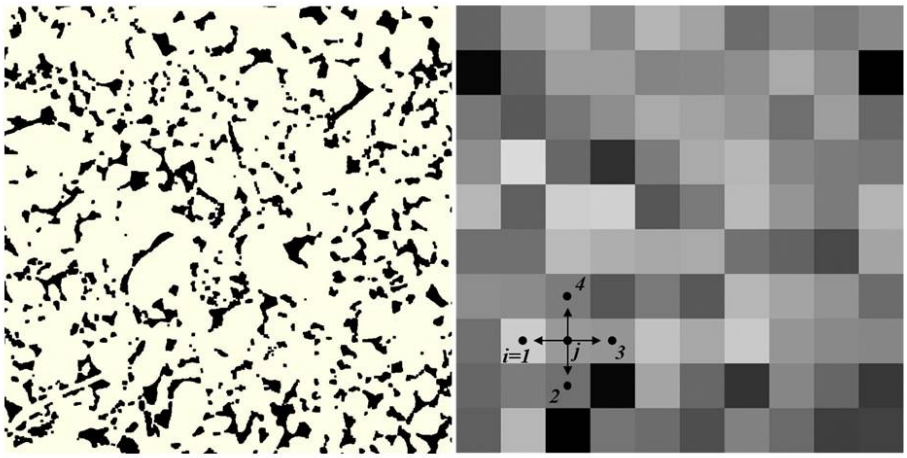

Figure B.1: Left: Numerical cross-section of a connected pore cluster obtained from a $d = 3$ dimensional XMT image (5 mm $\times$ 5 mm limestone sample), the black color indicates pore space. Right: Equivalent upscaled porosity map. The arrows indicate possible particle transitions to nearest neighbors.

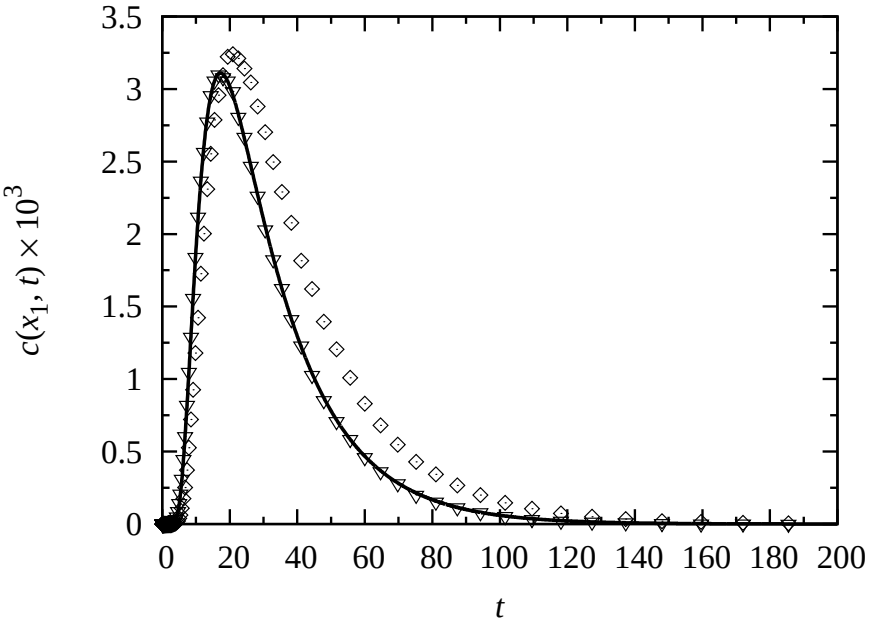

Figure B.2: Vertically averaged concentration at $x = 9$ m for diffusion in a heterogeneous medium characterized by a log-normally distributed diffusion coefficient. Comparison of the numerical solutions for interpixel diffusion coefficients given by the (squares) harmonic and (triangles) geometric mean, and the (solid line) analytical solution (41) with $D_G = 0.52$ m^{2}s^{-1}, and $L = 10$ m. The number of pixels used in the TDRW simulation in horizontal direction is 10^2 and in vertical direction 50. The simulations were performed using $N = 5 \times 10^8$ particles.

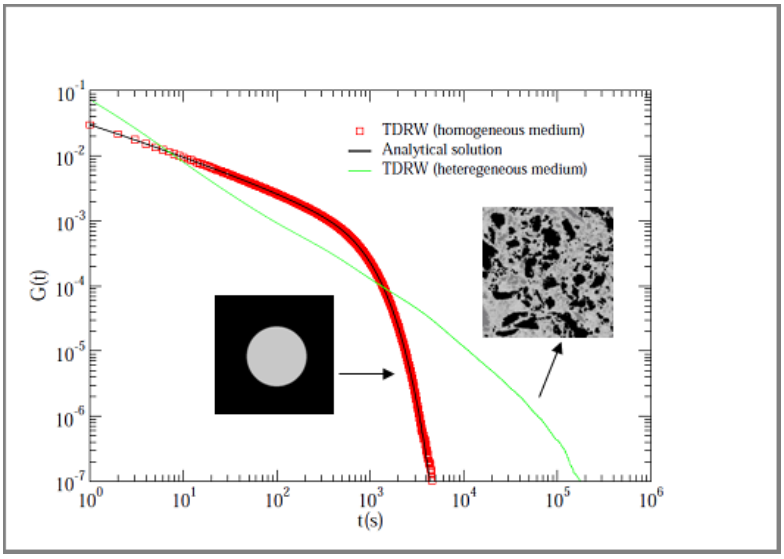

Figure B.3: Residence time distribution $\varphi(t)$ for a homogeneous sphere, and for a heterogeneous limestone sample as obtained from the TDRW simulation.

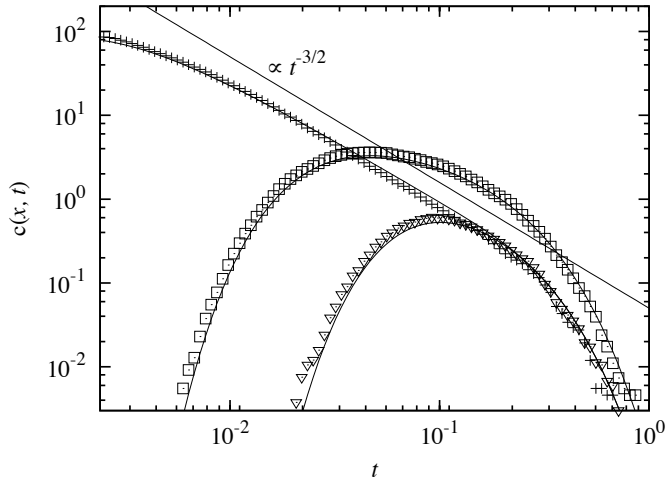

Figure B.4: Evolution of solute concentration in an heterogeneous $d = 1$ dimensional domain at three different observation points: $x = 0.1$ (crosses), $x = 0.5$ (squares), and $x = 0.9$ (triangles), compared with solution (41) of the equivalent homogeneous model (53) with $\phi_A = 0.48$ and $\phi_H = 0.43$.

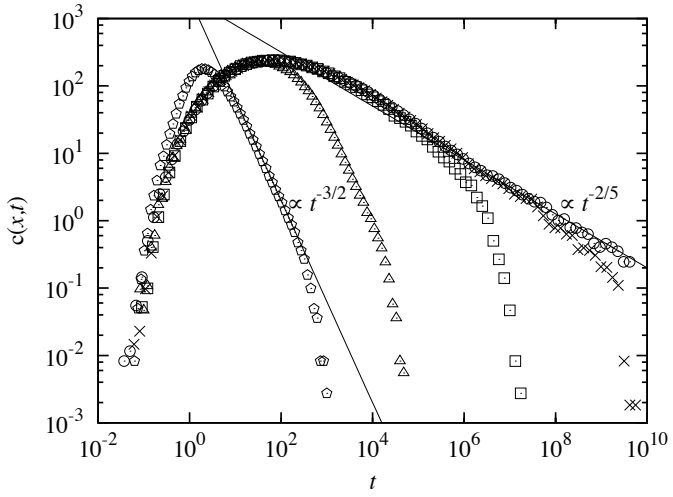

Figure B.5: Evolution of solute concentration in an heterogeneous $d = 1$ dimensional at $x = 0.1$ for the truncated power-law trapping time distribution (55) with $\beta = 0.4$ for cut-off times of (pentagons) $t_1 = 1$, (triangles) $t_1 = 10^3$, (squares) $t_1 = 10^7$, (crosses) $t_2 = 10^{10}$ and (circles) $t_2 = \infty$.